AIAA'88

AIAA-88-0529

Prediction of Induced Roll on Conventional Missiles with Cruciform Fin Sections

D. J. Lesieutre, M. R. Mendenhall, M. F. E. Dillenius, Nielsen Engineering & Research, Inc., Mountain View, CA

AIAA 26th Aerospace Sciences Meeting

January 11-14, 1988/Reno, Nevada

PREDICTION OF INDUCED ROLL ON CONVENTIONAL MISSILES WITH CRUCIFORM FIN SECTIONS

by

Daniel J. Lesieutre*
Michael R. Mendenhall**
Marnix F. E. Dillenius+
Nielsen Engineering & Research, Inc.
Mountain View, CA 94043

Abstract

The MISSILE 3 engineering prediction method for missile aerodynamic performance calculations has been improved to better predict missile longitudinal and lateral-directional forces and moments as well as individual fin forces and moments. The method considers nonlinear effects such as induced rolling moments due to the influence of asymmetric canard and body vorticity on missile tail fins. In addition, comparisons with experiment at transonic ($0.8 \leq M_\infty \leq 1.2$) and high Mach numbers ($M_\infty > 4$) and high angles of attack ($\alpha \leq 45°$) indicate that this prediction method is applicable to extreme flight conditions. Recent modifications to the MISSILE 3 code are described, and a number of measured and predicted aerodynamic characteristics are provided to demonstrate the capabilities and limitations of this lastest version.

Nomenclature

AR	aspect ratio of two fins joined at the root chord
C_l	rolling-moment coefficient; rolling moment/$q_\infty S_R l_R$, positive clockwise looking forward
C_m	pitching-moment coefficient; pitching moment/$q_\infty S_R l_R$, positive nose up
C_N	normal-force coefficient; normal force/$q_\infty S_R$
C_n	yawing-moment coefficient; yawing moment/$q_\infty S_R l_R$, positive nose to right
C_Y	side-force coefficient; side force/$q_\infty S$, positive to the right
D	maximum body diameter
i	fin number, i = 1,2,3,4, numbered clockwise looking forward; fin 1 of the first fin section is always in the first quadrant
l_R	reference length, D
M_∞	freestream Mach number
q_∞	freestream dynamic pressure
S_R	reference area, $\pi D^2/4$
α_c	body incidence angle
δ_i	fin deflection angle
Γ	vortex strength
λ	fin taper ratio
ϕ	body roll angle

Introduction

The MISSILE 3 engineering prediction method[1,2] is a data base prediction method based on an extensive systematic fin force and center of pressure data base. In concept the MISSILE 3 prediction method is similar to the previous data base prediction methods, MISSILE 2A[3,4] and MISSILE 2[5,6]; however, the new data base has a much larger scope in Mach number, angle of attack, aspect ratio, and control fin deflection angle, and the equivalent angle of attack concept has been improved. The range of flow conditions of the new fin-on-body data base and prediction method are $0.6 \leq M_\infty \leq 4.5$, $0° \leq \alpha_c \leq 45°$, $0° \leq \phi \leq 90°$, and $-40° \leq \delta_i \leq 40°$. The range of fin geometries allowed by the method is $0.25 \leq AR \leq 4.0$ and $0.0 \leq \lambda \leq 1.0$. The range of the method and allowed fin planform geometries are depicted in Fig. 1. The coordinate systems and sign conventions used by MISSILE 3 are shown in Fig. 2.

A previous paper[1] demonstrated that MISSILE 3 predicts the longitudinal aerodynamic characteristics of conventional missiles for angles of attack up to 25 degrees and Mach numbers less than 3.7. The purpose of the effort described in this paper is to illustrate the capability of the method to predict induced roll characteristics of conventional missiles at moderate to high angles of attack, $\alpha_c \leq 45°$, and Mach numbers from 0.8 to 4.6. The major features and components modeled by the prediction method for missiles at high angles of attack are illustrated in Fig. 3.

The prediction of missile lateral-directional aerodynamic characteristics is very difficult for any prediction method because of the dominating effects of canard trailing vorticity and afterbody vorticity on a missile's tail fins. This is particularly a problem for canard-controlled missiles at low angles of attack with roll or yaw control fin deflections. An asymmetric flow field develops near the tail fins because of the asymmetric canard loading and associated trailing vorticity. Induced roll is a consequence of this flow condition, and the problem is further complicated at high angles of attack because of afterbody separation which also influences the flow field in the tail fin region. Prediction of induced rolling moments under extreme flow conditions, including both canard trailing vortices and shed afterbody vortices, is a severe test of the capability of any missile aerodynamic prediction method.

This paper includes a brief description of recent improvements in the procedures for tracking afterbody vortices and calculating vortex influence on tail fins. Comparisons of measured and predicted aerodynamic characteristics are presented to demonstrate the capabilities and limitations of the method, and some details of the vortex flow phenomena considered by the method are shown to help explain the nonlinear results.

Technical Discussion

Though the primary intent of this paper is to present further verification of the MISSILE 3 prediction method, a brief description of several recent technical improvements i the method is included. The complete technical approach is presented in Ref. 1 and 2, and the following paragraphs serve to document recent changes in the calculation procedures.

* Research Engineer, Member AIAA
** Vice President, Associate Fellow AIAA
+ Director of Missile and Store Separation Aerodynamics, Associate Fellow AIAA

It should be emphasized here that the approach described is an engineering prediction method developed to predict complex flow-induced effects for a wide range of configurations and flow conditions.

The initial version of MISSILE 3 did not predict lateral-directional aerodynamic characteristics well. These characteristics are very sensitive to external flow conditions at all angles of attack, but a possible source of the prediction difficulties was found in the vortex flow model. The following describes the vortex flow model and its modifications.

Vortex Induced Flows

The vortex flow model included in MISSILE 3 is shown in the sketch in Fig. 4. In a plane normal to the missile axis, a single trailing vortex from a canard fin is shown as a point vortex outside the missile body. To satisfy boundary conditions on the missile surface, an image vortex is placed at the image point inside the body. To satisfy the boundary conditions at infinity, a vortex is also required at the center of the body. This is a common two-dimensional image model of a free vortex in the vicinity of a solid body.

Consider some of the flow conditions which can develop in a typical calculation. If the canard fin vortex moves a large distance from the body, its effect on the induced loads on the missile should decrease, and in the limit approached as the external vortex moves to infinity, its effect decreases to zero. This is what happens with the above flow model: as the external vortex moves away from the body, the image vortex moves toward the center of the body where in the limit it is exactly cancelled by the center vortex, and there is no resulting swirl in the flow.

In the other flow condition, the external vortex is near the body. In this case, the effect of the external vortex and its image are additive in the vicinity of the body, but they are counteracted by the center vortex. This results in an underestimation of the amount of swirl in the flow.

If the center vortex is omitted from the flow model (which appears to be the best model for vortices generated on the body and attached to the body by a feeding sheet), the two flow conditions described above have entirely different characteristics. When the canard vortex is near the body, its effect is added to that of the image vortex, and the major vortex-induced loads are concentrated locally on the body and the fins. When the vortex moves away from the body toward infinity, the image vortex moves to the center of the body, and, as described above, it induces an unbalanced swirling flow and associated rolling moment.

Based on observation and comparison with experiment, no single flow model is appropriate for all conditions; therefore, a combination of flow models with a transition or matching region is required. An attempt to tailor a center vortex model to represent experimentally observed induced effects was made with some success. This model weights the center vortex such that its effect disappears when the external vortex is in close proximity to the body surface, but when the vortex moves away from the body, the center vortex is at full strength in order to produce the non-swirling flow field described above. Preliminary results indicate that when the external vortex is one diameter from the body surface, the center vortex model begins to have a significant role in the calculation. All results from MISSILE 3 presented in this paper were obtained with this modified vortex model.

Body Separation

An additional area of concern in this investigation was the body vortex shedding and tracking used in MISSILE 3 for asymmetric flow conditions. Program MISSILE 3 specifies the separation point on the body as a function of cross flow Mach number (based on experimental data). This is done to avoid the computational expense of having to predict the separation points based on the pressure distribution. The separation points are taken to be symmetric with respect to the cross flow velocity vector regardless of whether there are upstream asymmetries. However, the shed vortices on each side of the body can have different strengths because they are based on local flow conditions at the separation points. Therefore, upstream asymmetric flow conditions result in asymmetric vortices shed from the left and right sides of the body, thus yielding a side force, yawing moment, and asymmetric flow conditions in the tail fin region.

The previous data base prediction method MISSILE 2A[5] and a supersonic body-alone prediction method NOZVTX[7] both predict the separation point locations and then determine the strength of the shed vorticity. To test if the results produced by MISSILE 3 are reasonable, NOZVTX was run to simulate the tracking and shedding of vorticity on the afterbody of an AIM9 type missile.[8] The strength and locations of the canard vortices were input as initial conditions. The test case corresponds to the AIM9 at $\alpha = 15^\circ$, $\phi = 0^\circ$, $M_\infty = 2.5$, and $\delta_{2,4} = \pm 5^\circ$ for roll control. The tracking tolerance and the vortex core size were forced to be identical in the two codes. The only difference between the two cases was the location of the body separation points.

Figure 5 illustrates the differences in predicted vortex characteristics at the tail root chord leading edge. The canard vortices are shown at the top of the figure. The tracking of the canard fin trailing vorticity is essentially identical in MISSILE 3 and NOZVTX. The strength and locations of the body vorticity (centroids) are also in reasonable agreement. These results give some confidence that the body vortex shedding and tracking model in MISSILE 3 is sufficient to represent asymmetric nonlinear effects.

Results

Comparisons of measured and predicted aerodynamic performance of a number of conventional missiles are presented in this section. Examples of the longitudinal aerodynamic predictions are shown, followed by the lateral-directional aerodynamic predictions for roll and/or yaw control deflections. In addition to the MISSILE 3 results, results are included from the preliminary analysis and design code Missile Datcom[9] (MISDAT) to provide an indication of the available capabilities in missile aerodynamic prediction. It is not the purpose to evaluate MISDAT in this paper, but results from the method are presented to provide a standard with which to compare MISSILE 3. It should be noted that Missile Datcom does not currently include effects of body vorticity.

Measured and predicted results on a canard-body-tail configuration[10] are shown in Figs. 6 and 7. The model has a 7.6 diameter forebody, four canard fins

with aspect ratio 2.7 and taper ratio 0.20, an afterbody of 5.6 diameters, and four cruciform tail fins with aspect ratio 2.6 and taper ratio 0.0. Figure 6 shows longitudinal pitch control results for $\phi = 45^\circ$ at $M_\infty = 2.0$ and 4.6. Figure 7 illustrates lateral-directional results on the same missile with canard roll control deflections for $\phi = 45^\circ$ at $M_\infty = 2.0$ and 4.6.

Figure 6(a) demonstrates the longitudinal prediction capabilities for $M_\infty = 2.0$, $\phi = 45^\circ$, and angles of attack up to 45 degrees. The MISSILE 3 normal force results are in good agreement with measured results for all angles of attack with no pitch deflections. When all of the canard fins are deflected 10 degrees for pitch control ($\delta_i = 10^\circ$), the MISSILE 3 predicted normal force and measured normal force agree well at low and very high angles of attack but are slightly underpredicted in the intermediate range. Note that the predicted results with and without pitch deflections do not converge at the very high angles as the experimental data does.

The pitching moment comparison in Fig. 6(a) indicates that MISSILE 3 predicts the effect of pitch control at low and very high angles of attack. Through the intermediate angles of attack, $12^\circ \lesssim \alpha_c \lesssim 24^\circ$, there is a dip in the pitching moment prediction. This dip is due primarily to a difference in the nose and tail fin force contributions to the pitching moment. At small angles of attack the tail fins dominate the pitching moment because there is no afterbody vorticity, the canard fin vortices are small, and the nose force is small. The location of the canard fins with respect to the moment center minimize their contribution to the pitching moment. In the intermediate angle of attack range, the predicted nose force is growing at a larger rate than the predicted tail force, thus causing the dip in the pitching moment curve. At intermediate angles of attack, the canard vortices become significant and pass close to the tail fins causing the tail fins to become unloaded and allowing the nose force to dominate the pitching moment. It should be noted that the experimental data show a similar but less pronounced variation in the pitching moment for $5^\circ \lesssim \alpha_c \lesssim 16^\circ$ when the canard fins are not deflected. At the higher angles of attack, the canard vortices move up and far away from the tail fins allowing them to load up and again dominate the pitching moment as at the lower angles of attack.

Figure 6(b) demonstrates the longitudinal prediction capabilities at $M_\infty = 4.6$, $\phi = 45^\circ$, and angles of attack up to 45 degrees. The MISSILE 3 normal force and pitching moment results agree well with measured results for all angles of attack with no canard fin pitch deflections. When all of the canard fins are deflected 20 degrees for pitch control ($\delta_i = 20^\circ$), the predicted and measured normal force results agree well to $\alpha_c = 30^\circ$. The predicted pitching moment for the deflected case shows the correct trend but underpredicts the magnitude. Both MISSILE 3 and MISDAT predict longitudinal aerodynamic characteristics reasonably well.

Figure 7(a) shows predicted and measured results for $M_\infty = 2.0$, $\phi = 45^\circ$, and canard fins 1 and 3 deflected -10° and $+10^\circ$, respectively, for right fin down roll control. The side force and yawing moment are not of much interest in this case, especially if they are put into perspective with respect to the normal force and pitching moment. MISSILE 3 predicts the rolling moment well for angles of attack up to 20 degrees, but it does not predict the magnitude at the very high angles of attack. Near $\alpha_c = 0^\circ$ the total rolling moment is determined from the canard fins with roll control deflections and from the induced rolling moment of the tail fins under the influence of the asymmetric vortices from the canards. At $\alpha_c = 0^\circ$ MISSILE 3 predicts the canard fin section contribution to the rolling moment to be 1.33 and the tail fin section contribution to be -0.37. The total rolling moment is the sum, which agrees well with the measured results. Results predicted by MISDAT generally underestimate the rolling moment.

Also shown as part of Fig. 7(a) are the vortex fields predicted by MISSILE 3 at several angles of attack. These fields are shown in a crossflow plane at the tail fin root chord leading edge. It is seen that the asymmetric canard fin vortices due to roll control deflections cause asymmetric body vorticity. The fin vortices from canard fins 2 and 3 have a strong influence on tail fins 2 and 3 for angles of attack less than 15 degrees and have a strong effect on tail fins 1 and 4 for angles between 15° and 35°. Also of interest is that the body vorticity rolls up under its own influence at the low and moderate angles of attack, but at the very high angles, the vortex tracking seems to be dominated by the high cross flow velocity. This is seen at $\alpha_c = 44^\circ$ where the body vortices move up and toward the body centerline.

Figure 7(b) shows predicted and measured results for $M_\infty = 4.6$, $\phi = 45^\circ$, and canard fins 1 and 3 deflected -10° and $+10^\circ$, as for the $M_\infty = 2.0$ case discussed above. MISSILE 3 predicts the rolling moment trends for angles of attack up to 30 degrees, but it does not predict the magnitude or trend at the very high angles of attack. Program MISDAT predicts near constant rolling moment. The break over of the measured rolling moment at angles above 24 degrees is difficult to predict and is probably beyond the scope of most preliminary design methods because of the very high cross flow mach number.

Measured and predicted results on the canard-body-tail configuration[8] depicted in Fig. 8 are shown in Figs. 8 - 11. The model has a 3.73 diameter forebody, four canard fins with aspect ratio 2.0 and taper ratio 0.3, an afterbody of 12.7 diameters, and four cruciform tail fins with aspect ratio 1.06 and taper ratio 0.58. Longitudinal results are given first, and they are followed by lateral-directional results for roll and yaw canard control fin deflections.

Figure 8 contains longitudinal pitch control results at $M_\infty = 2.5$ for $\phi = 0^\circ$ and 45°. Figure 8(a) shows predicted and measured results for $\phi = 0^\circ$ and canard fins 2 and 4 deflected 0° and 5° for pitch control. MISSILE 3 predicts the correct effect of pitch deflection on both the normal force and pitching moment. The normal force is slightly underpredicted at the higher angles of attack. Figure 8(b) shows predicted and measured longitudinal results for $\phi = 45^\circ$. The predicted normal force is less than the measured results above $\alpha_c = 10^\circ$ for reasons as yet unknown.

Figure 9 depicts measured and predicted results at $M_\infty = 2.5$ for $\phi = 0^\circ$ and 45° with canard fins 2 and 4 deflected $+5^\circ$ and -5°, respectively, for roll control. Figure 9(a) shows predicted and measured lateral-directional results for $\phi = 0^\circ$. This roll control case has been investigated previously by Dillenius et al[11] with the panel code prediction method NSWCDM and by Allen and Townsend[12] with the finite difference

Euler code SWINT. These predicted results are shown in addition to the MISSILE 3 and Missile Datcom results.

MISSILE 3 and MISDAT do a reasonable job of predicting the rolling moment without tail fins. For the complete configuration, the induced roll on the tail fins at small angles of attack is due to the influence of the asymmetric canard vortices. At the higher angles of attack, the body vorticity has a large effect on the rolling moment, as noted by Dillenius,[10] because of the long afterbody of this missile. MISSILE 3 predicts the rolling moment trend but predicts the turn around in the rolling moment at higher angle of attack than the experiment.

At the higher angles of attack, the canard fin vortices move away from the tail fins and do not have much influence. The body vorticity is the dominating effect as illustrated by the difference in the MISSILE 3 results with (solid curve) and without (dashed curve) afterbody vorticity. The SWINT results from Ref. 12 are limited to angles of attack for which there are no subsonic pockets on the missile and do not include asymmetric afterbody shedding. Program MISDAT predicts the rolling moment without tail fins adequately but overestimates the complete configuration rolling moment.

Also shown as part of Fig. 9(a) are predicted vortex fields from MISSILE 3 at the beginning of the tail section for several angles of attack. It is obvious that the asymmetric canard fin vortices due to roll deflection cause asymmetric body vorticity. For angles of attack exceeding 16 degrees, the highly loaded canard vortices have minimal influence on the tail fins; therefore, the afterbody vorticity influences the tail fins to produce a large induced rolling moment. It is seen in the vortex fields that, as the angle of attack increases, the body vortex asymmetries increase and actually break away from their feeding sheets to form a vortex street effect.

Figure 9(b) illustrates predicted and measured results for $M_\infty = 2.5$, $\phi = 45^\circ$, and canard fins 2 and 4 deflected $+5^\circ$ and -5°, respectively, for roll control. Both MISSILE 3 and MISDAT predict the tail fin off rolling moment well. The complete configuration results are similar to the previous results at $\phi = 0^\circ$ in the sense that MISSILE 3 predicts the correct trend in the rolling moment, but it does not predict the turn around until a higher angle of attack. The effect of the afterbody vorticity on the induced rolling moment on the tail fins is also apparent for this configuration rolled to $\phi = 45^\circ$.

Figure 10 shows the effect of canard fin roll control at $\phi = 26.6^\circ$ for $M_\infty = 1.75$ and 2.5. Figure 10(a) shows predicted and measured results at $M_\infty = 1.75$ with canard fins 2 and 4 deflected $+5^\circ$ and -5°, respectively, for roll control. As with the previous roll control results for this configuration, the tail fin off rolling moment predictions agree with the measured data. MISSILE 3 does a reasonable job of predicting the complete configuration rolling moment but exaggerates the yawing moment. The reason for this problem has not been fully determined, but one contribution is from the right horizontal canard fin 2 vortex passing very near the upper tail fin 1.

Figure 10(b) shows predicted and measured results on the same configuration at $M_\infty = 2.5$ and $\phi = 26.6^\circ$ with roll control. As with the previous $M_\infty = 2.5$ results in Fig. 9, the rolling moment prediction is reasonable. A comparison of Fig. 10(a) and 10(b) indicates that both the experimental results and the MISSILE 3 predictions show a significant Mach number effect on the rolling moment. The tail fin off rolling moment prediction agrees with the measured results, and the side force and yawing moment predictions are much better than the $M_\infty = 1.75$ results. Program MISDAT tends to overestimate the rolling moment but predicts the yawing moment better than MISSILE 3.

Figure 11 shows predicted and measured results for $M_\infty = 2.5$, $\phi = 0^\circ$, and canard fins 1 and 3 deflected 5 degrees for yaw control. The overall characteristics of the yawing moment and induced rolling moment are predicted well by MISSILE 3 and MISDAT except at the higher angles of attack. A problem encountered with these calculations is caused by the canard fin 3 vortex passing very close to the body. This problem is not apparent in the results discussed below for yaw control deflection of 20 degrees.

Included as part of Fig. 11 are the vortex fields at the beginning of the tail fin section predicted by MISSILE 3 for several angles of attack. It is again seen that the asymmetric canard fin vortices due to yaw control deflections cause asymmetric body vorticity. As important as the body vorticity in this case is the fact that the windward canard fin vortex, loaded due to yaw deflection, travels very near the body at low angles of attack, very near the body and tail fin 2 at low and moderate angles of attack, and very near the leeward body vorticity at moderate angles of attack. This individual vortex can have a strong influence on the lateral-directional characteristics. The following results with 20 degrees yaw deflections do not have a similar problem with the windward fin vortex because the vortices are displaced further from the body centerline due to the larger deflection angle.

Measured and predicted results on the canard-body-tail configuration[13] depicted in Fig. 12 are shown in Figs. 12 and 13. This model, similar to the configuration shown in Fig. 7, has a 2.0 diameter forebody, four canard fins with aspect ratio 3.8 and taper ratio 0.06, an afterbody of 13.5 diameters, and four cruciform tail fins with aspect ratio 0.87 and taper ratio 0.64. Transonic yaw control results are presented for $M_\infty = 0.8$ and 1.14. These data provide longitudinal and lateral-directional characteristics when the control fins are deflected for yaw; however, there are slight experimental errors due to sting deflections for which the data have not been corrected. These errors may change the magnitude of the measured results slightly, but they should not significantly alter the experimental trends. It should be emphasized that MISSILE 3 uses an extensive transonic control fin-on-body fin normal-force coefficient data base to get the fin deflection effect in the transonic speed regime.

Figure 12 shows predicted and measured results for $M_\infty = 0.8$, $\phi = 0^\circ$, and with canard fins 1 and 3 deflected 20 degrees for yaw control. The longitudinal aerodynamic characteristics are shown in Fig. 12(a), and the lateral-directional results are shown in Fig. 12(b). The predicted longitudinal results agree well with the measured results over the entire angle of attack range. The side force in Fig. 12(b) is not in good agreement. The predicted yawing moment trend is in reasonable agreement with experiment, but it is underestimated in the same angle region where the side force is not predicted well. MISSILE 3 does a

good job of predicting the induced rolling moment except for a slight underprediction of the maximum rolling moment. The MISSILE 3 results show no significant effect of afterbody vorticity on the side force, yawing moment, or rolling moment. Program MISDAT generally produces good predictions except for the rolling moment in the intermediate angle of attack range.

Included as part of Fig. 12 are predicted vortex fields at several angles of attack. The asymmetric canard fin vortices due to yaw control deflections cause asymmetric body vorticity. The windward canard vortex tracks further away from the body than the 5 degrees yaw control case previously described, but because of its larger strength, this vortex has a much more pronounced effect on the body lee-side vorticity.

Figure 13 shows predicted and measured results for $M_\infty = 1.14$, $\phi = 0^\circ$, and canard fins 1 and 3 deflected 20 degrees for yaw control. The longitudinal aerodynamic charactersistics are shown in Fig. 13(a), and the lateral-directional results are shown in Fig. 13(b). The predicted longitudinal results agree well with the measured results except at the higher angles of attack where the normal force is underpredicted. The side force and yawing moment predictions are similar to those at $M_\infty = 0.8$, but do not show as much effect of Mach number as the experimental results. The induced rolling moment predicted by MISSILE 3 agrees with the measured results well except for the maximum value, as was the case for $M_\infty = 0.8$. The body vorticity does not have as much of an effect for yaw control deflections as it does for roll control deflections. This is because the roll control deflections cause larger asymmetries in the body vortices shed from the left and right sides of the body.

Conclusions

The lastest version of the MISSILE 3 code has demonstrated the capability of predicting nonlinear vortex-induced aerodynamic characteristics of conventional missiles under extreme flow conditions of transonic and high Mach numbers and high angles of attack. The prediction of induced rolling moment is very good under a variety of flow conditions, but under certain flow conditions, the prediction of side forces and yawing moments is lacking.

The extensive systematic fin-on-body fin force and centers-of-pressure data bases used in the MISSILE 3 code, along with the nonlinear fin and body vortex modeling, provides an economical means to accomplish parametric studies of nonlinear aerodynamic forces and moments, both longitudinal and lateral-directional, during the preliminary design phase without resorting to more detailed aerodynamic analyses. Typical run times (VAX 11/750) for an angle of attack sweep can range from 2-5 minutes for a configuration without afterbody vortex shedding (or a body-tail configuration) to 15-30 minutes with afterbody shedding on a configuration with a long afterbody. The afterbody vortex shedding and tracking can be time consuming, but it is necessary for lateral-directional aerodynamic predictions based on results presented in this paper.

Acknowledgements

The effort reported herein was funded under a Nielsen Engineering & Research IR&D program. The authors gratefully acknowledge the assistance of the MISSILE 3 users who have discovered anomalies and assorted bugs in the early versions of the code.

References

[1]Lesieutre, D. J., Mendenhall, M. R., Nazario, S. M., and Hemsch, M. J.: "Aerodynamic Characteristics of Cruciform Missiles at High Angles of Attack," AIAA Paper 87-0212, January 1987.

[2]Lesieutre, D. J., Mendenhall, M. R., Nazario, S. M., and Hemsch, M. J.: "Prediction of the Aerodynamic Characteristics of Cruciform Missiles Including Effects of Roll Angles and Control Deflections," NEAR TR 360, August 1986.

[3]Hemsch, M. J. and Mullen, J., Jr.: "Analytical Extension of the MISSILE 1 and MISSILE 2 Computer Programs," NEAR TR 272, March 1982.

[4]Smith, C. A. and Nielsen, J. N.: "Prediction of Aerodynamic Characteristics of Cruciform Missiles to High Angles of Attack Utilizing a Distributed Vortex Wake," NEAR TR 208, January 1980.

[5]Nielsen, J. N., Hemsch, M. J., and Smith, C. A.: "A Preliminary Method for Calculating the Aerodynamic Characteristics of Cruciform Missiles to High Angles of Attack Including Effects of Roll Angle and Control Deflections," ONR-CR215-226-4F, November 1977.

[6]Hemsch, M. J., Smith, C. A., Nielsen, J. N., and Perkins, S. C., Jr.: "Calculation of Component Forces and Moments of Arbitrarily Banked Cruciform Missiles with Control Deflections," ONR-CR215-226-3, November 1976.

[7]Mendenhall, M. R. and Perkins, S. C., Jr.: "Prediction of Vortex Shedding From Circular and Noncircular Bodies in Supersonic Flow," NASA CR 3754, January 1984.

[8]Blair, A. B., Jr., Allen, J. M., and Hernandez, G.: "Effect of Tail Fin Span on Stability and Control Characteristics of a Canard Controlled Missile at Supersonic Mach Numbers," NASA TP 2157, June 1983.

[9]Vukelich, S. R., and Jenkins, J. E.: "Missile Datcom: Aerodynamic Prediction of Conventional Missiles Using Component Build-Up Techiniques," AIAA Paper 84-0388, January 1984.

[10]Monta, J. M.: "Supersonic Aerodynamic Characteristics of a Sparrow III Type Missile Model With Wing Controls and Comparison With Existing Tail-Control Results," NASA TP 1078, November 1977.

[11]Dillenius, M. F. E., Hemsch, M. J., Sawyer, W. C., Allen, J. M., and Blair, Jr., A. B.: "Comprehensive Missile Aerodynamics Programs for Preliminary Design," Journal of Spacecraft & Rockets, Vol. 20, No. 4, July-August 1983, pp. 414-416.

[12]Allen, J. M., and Townsend, J. L.: "Application of the SWINT Code to Wing/Body/Tail Geometries," AIAA Paper 85-1811, August 1985.

[13]Piper, E. M. and Brown A. E.: "AIM-9L Wind Tunnel Test Report," NWC TN 4036-233 Rev. 1, February 1974.

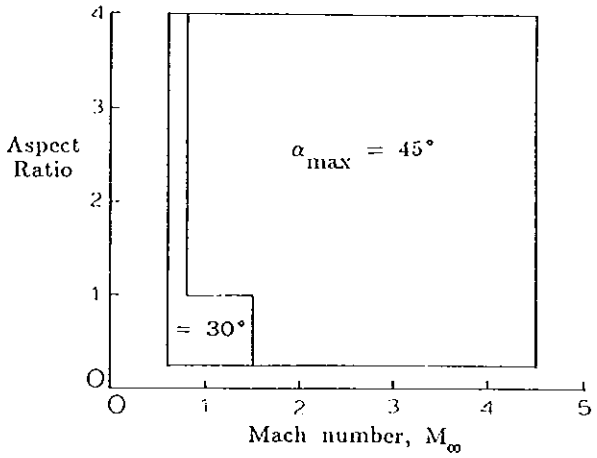

(a) Mach number, fin aspect ratio, and angle of attack range

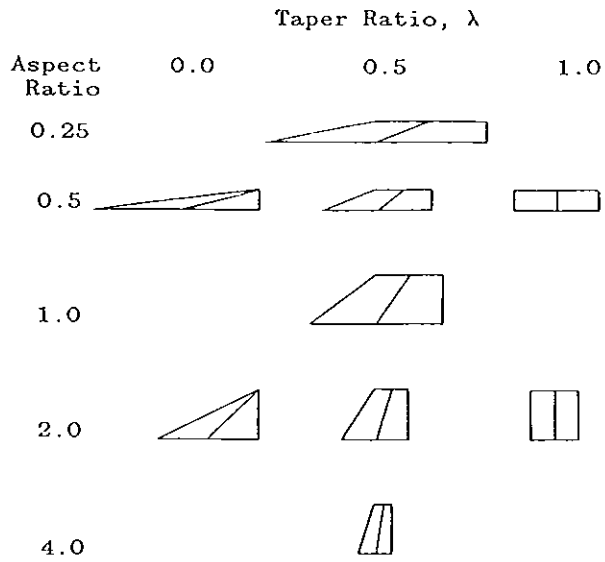

(b) Fin geometry characteristics

Figure 1.- Range of geometry and flow conditions of the MISSILE 3 prediction method.

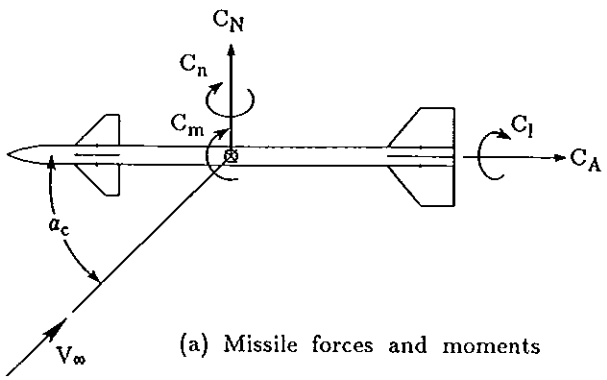

(a) Missile forces and moments

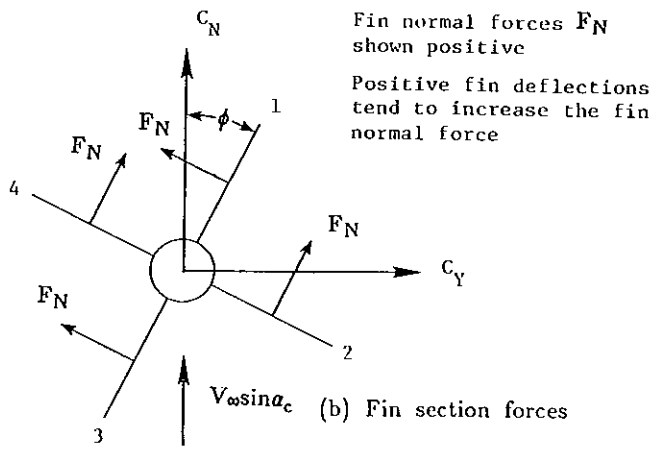

(b) Fin section forces

Figure 2.- Coordinate systems and sign conventions used by MISSILE 3.

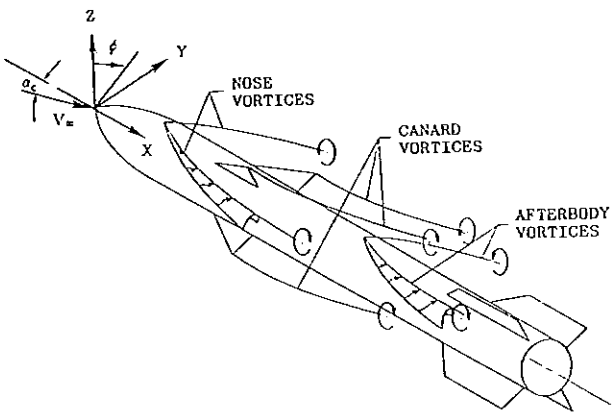

Figure 3.- Banked missile at angle of attack showing typical vortex field.

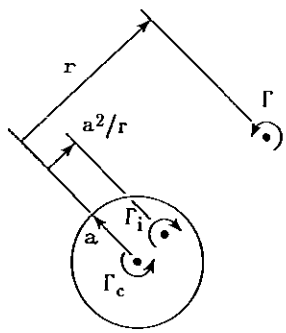

Figure 4.- External vortex flow model.

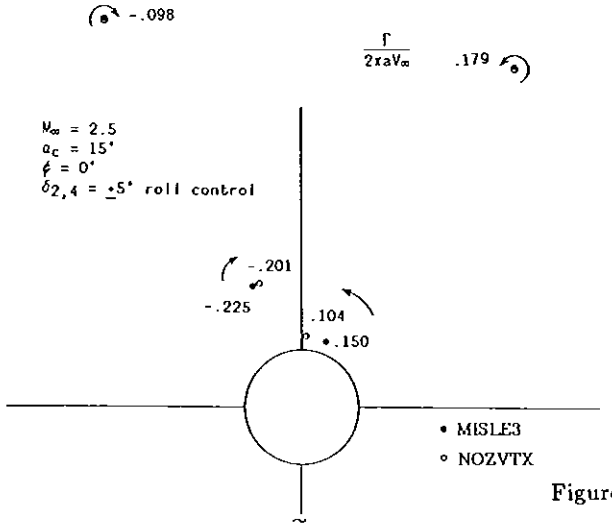

Figure 5.- Comparison of MISSILE 3 and NOZVTX body vortex shedding and tracking characteristics.

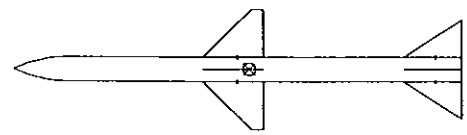

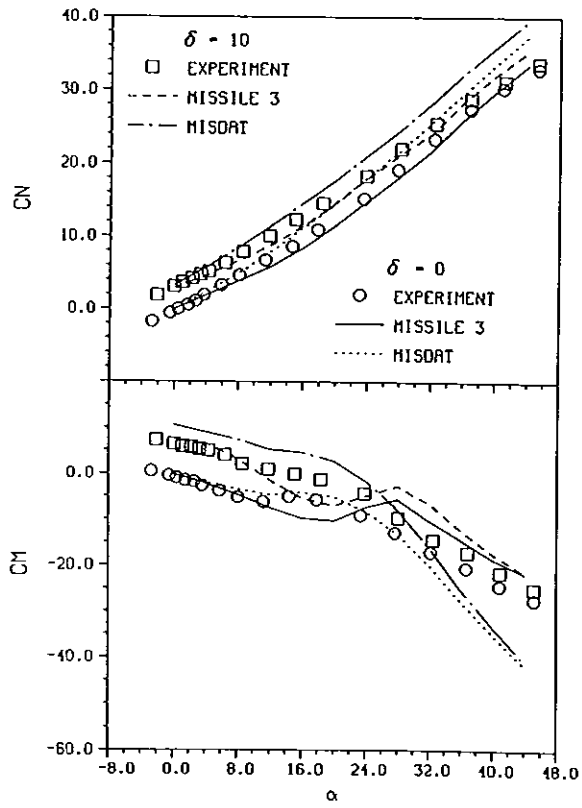

(a) $M_\infty = 2.0$

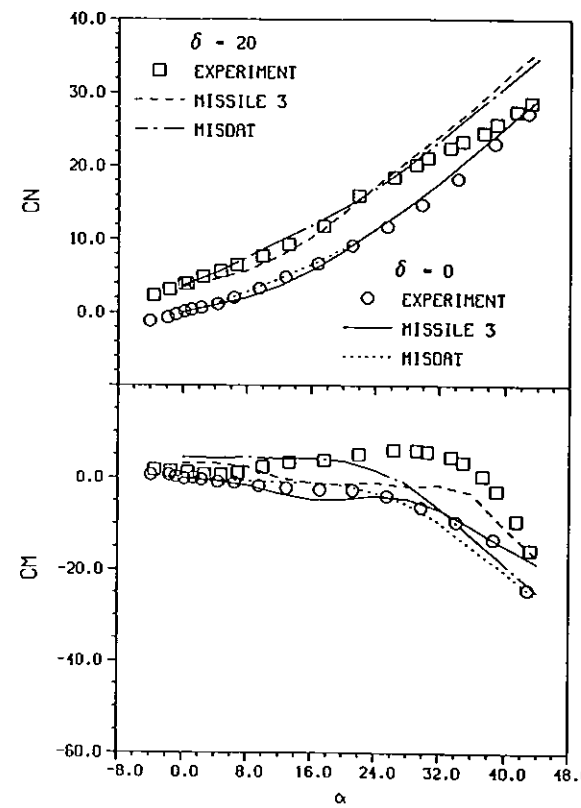

(b) $M_\infty = 4.6$

Figure 6.- Comparison of predicted and measured longitudinal aerodynamic characteristics for the canard-body-tail model in Ref. 10, $\phi = 45°$, all canard fins deflected for pitch control.

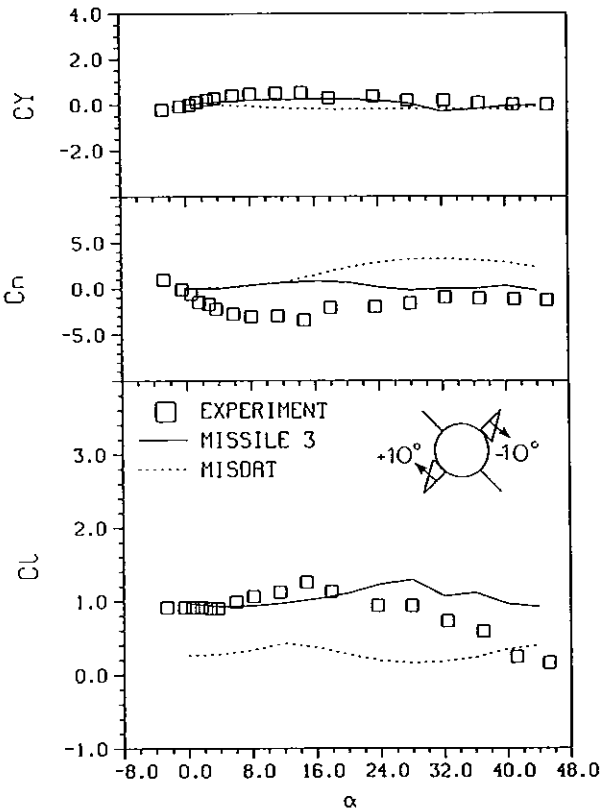

(a) $M_\infty = 2.0$

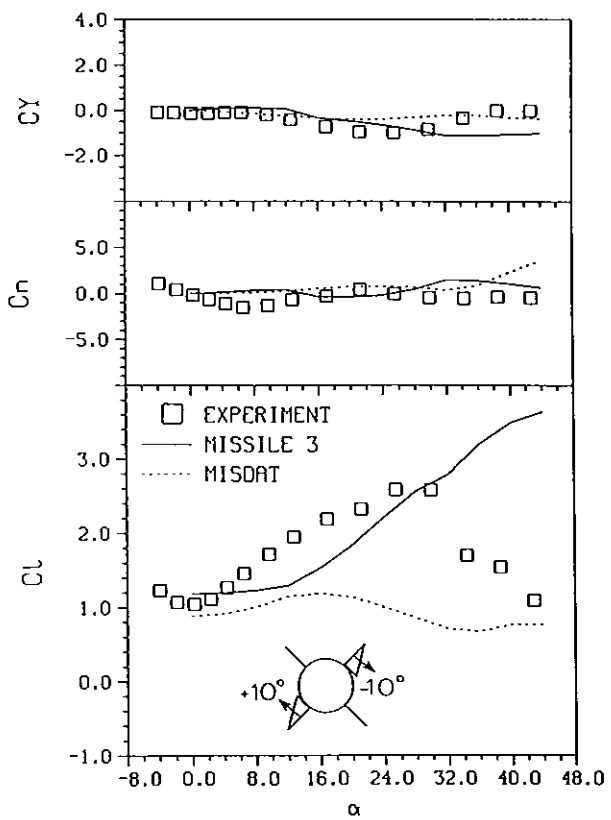

(b) $M_\infty = 4.6$

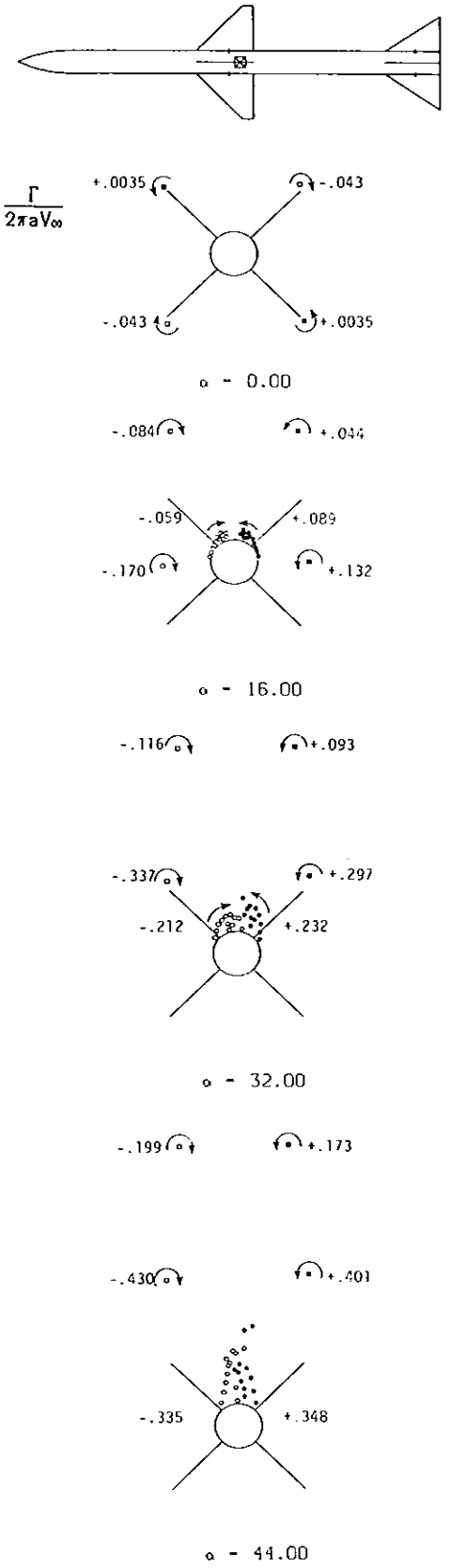

Figure 7.- Comparison of predicted and measured lateral-directional aerodynamic characteristics for the canard-body-tail model in Ref. 10, $\phi = 45°$, $\delta_{3,1} = \pm 10°$ roll control.

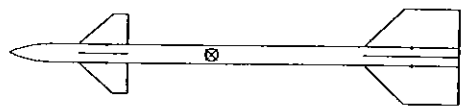

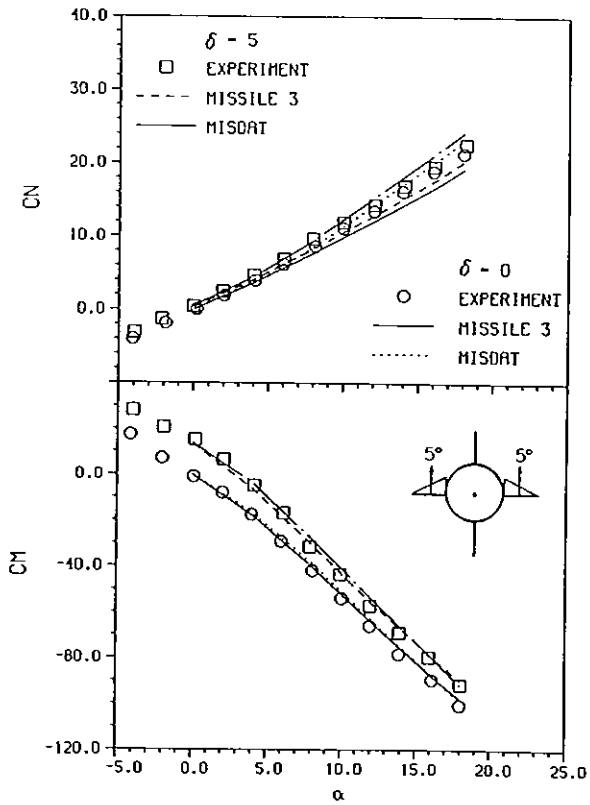

(a) $\phi = 0°$

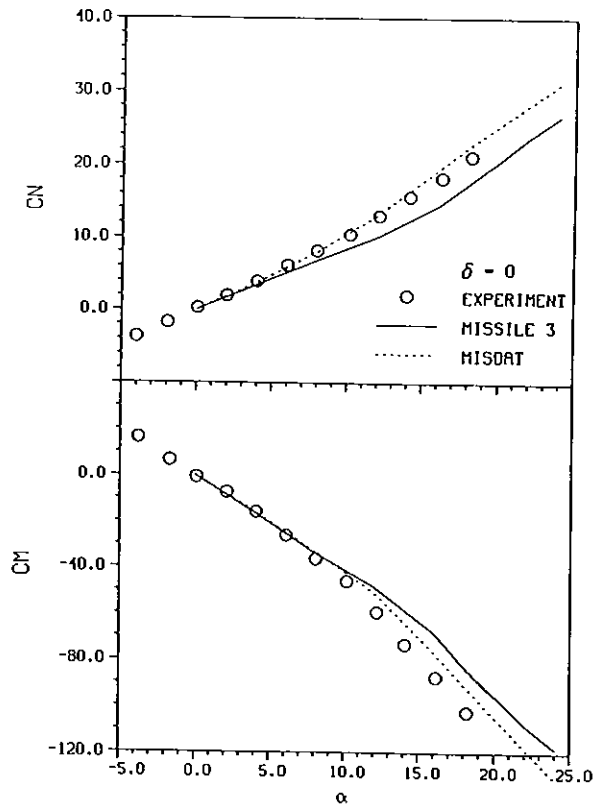

(b) $\phi = 45°$

Figure 8.- Comparison of predicted and measured longitudinal aerodynamic characteristics for the canard-body-tail model in Ref. 8, $M_\infty = 2.5$, canard fins 2 and 4 deflected for pitch control.

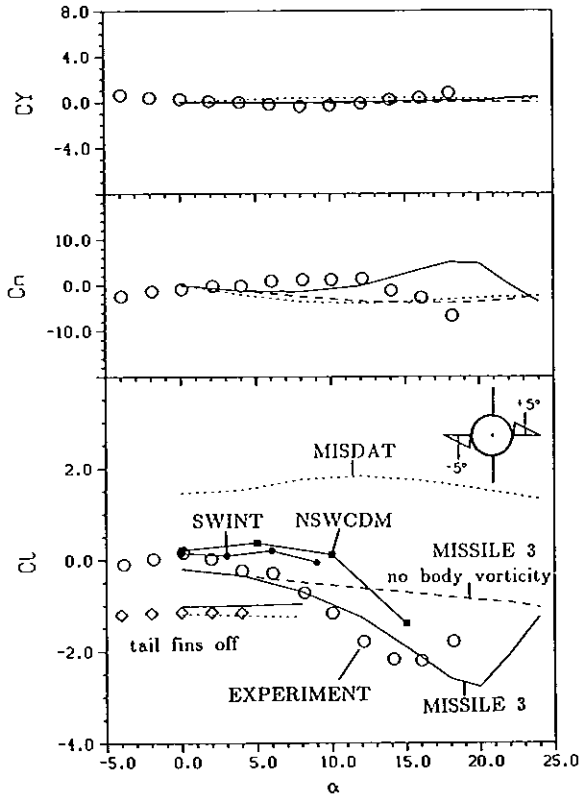

(a) $\phi = 0°$

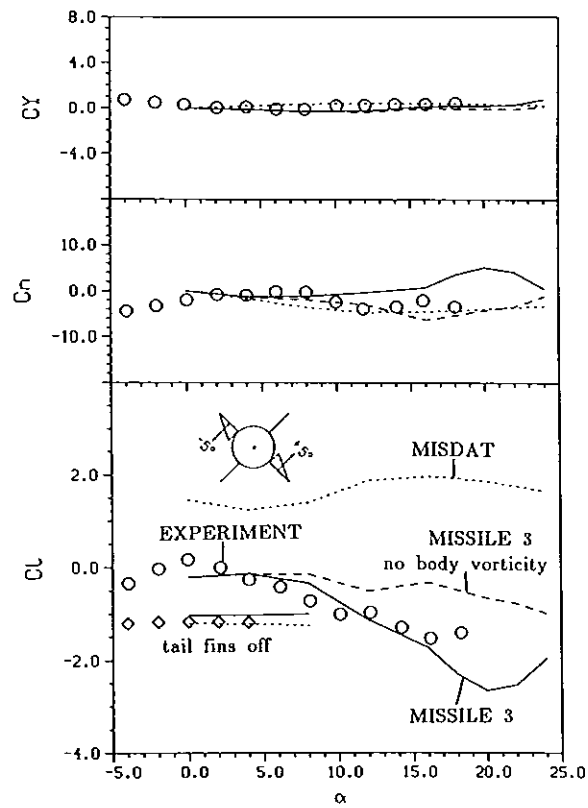

(b) $\phi = 45°$

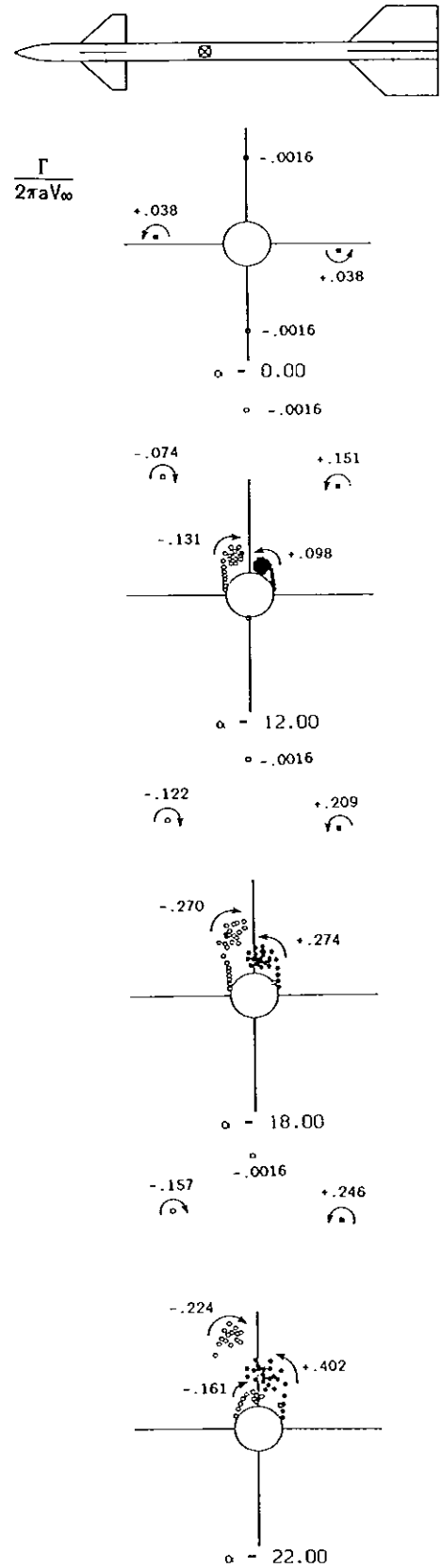

Figure 9.- Comparison of predicted and measured lateral-directional aerodynamic characteristics for the canard-body-tail model in Ref. 8, $M_\infty = 2.5$, $\delta_{2,4} = \pm 5°$ roll control.

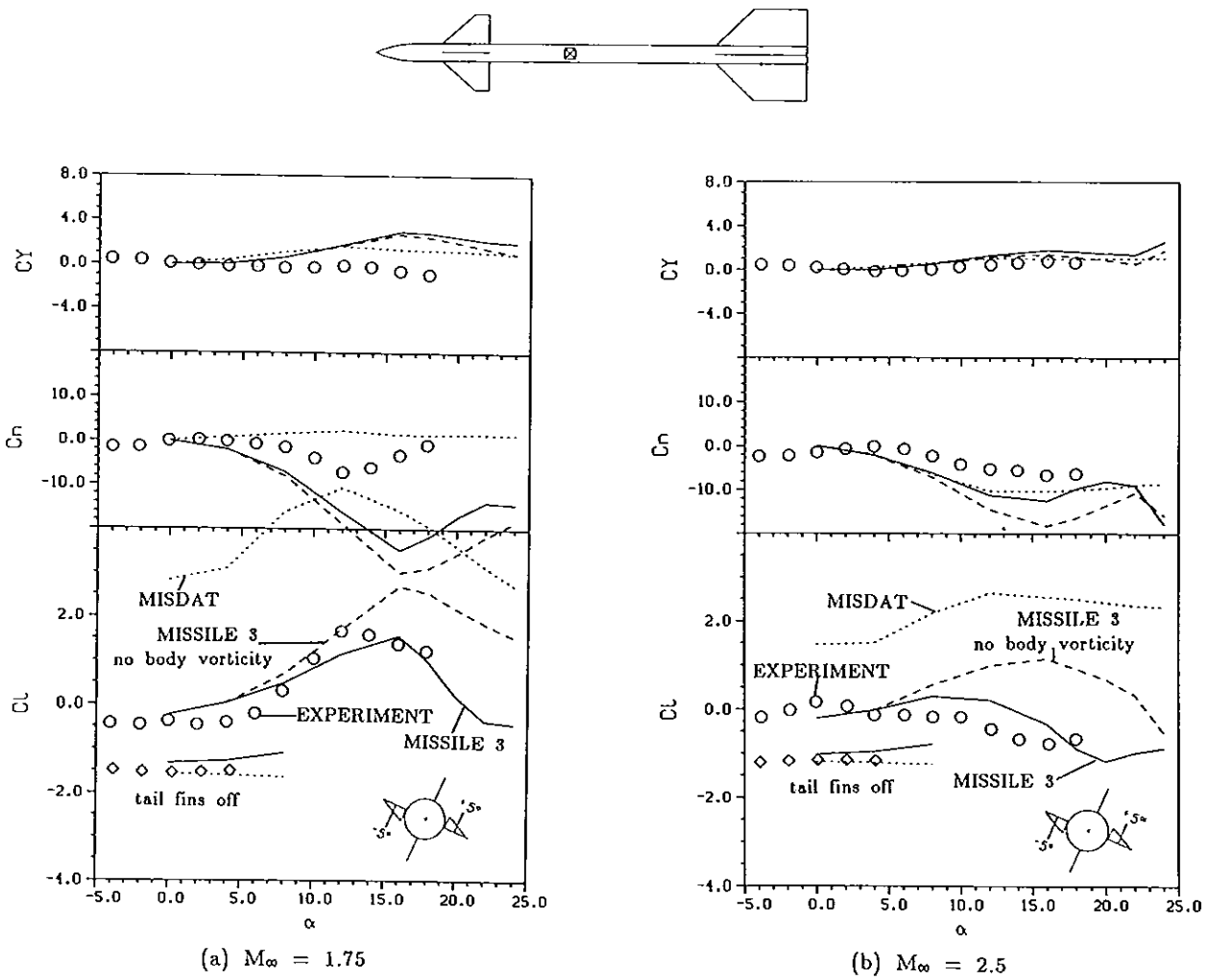

Figure 10.- Comparison of predicted and measured lateral-directional aerodynamic characteristics for the canard-body-tail model in Ref. 8, $\phi = 26.6°$, $\delta_{2,4} = \pm 5°$ roll control.

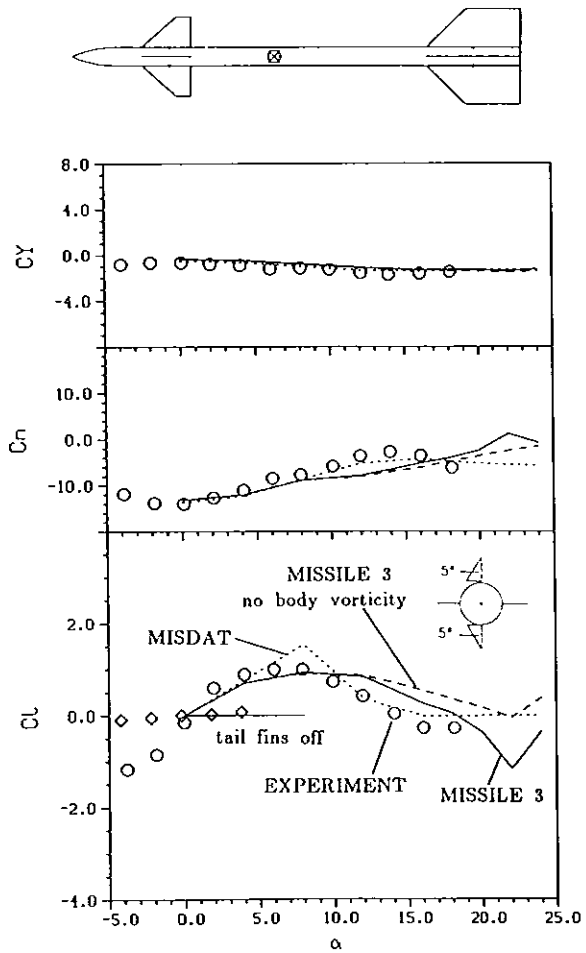

Figure 11.- Comparison of predicted and measured lateral-directional aerodynamic characteristics for the canard-body-tail model in Ref. 8, $M_\infty = 2.5$, $\phi = 0°$, $\delta 1,3 = 5°$ yaw control.

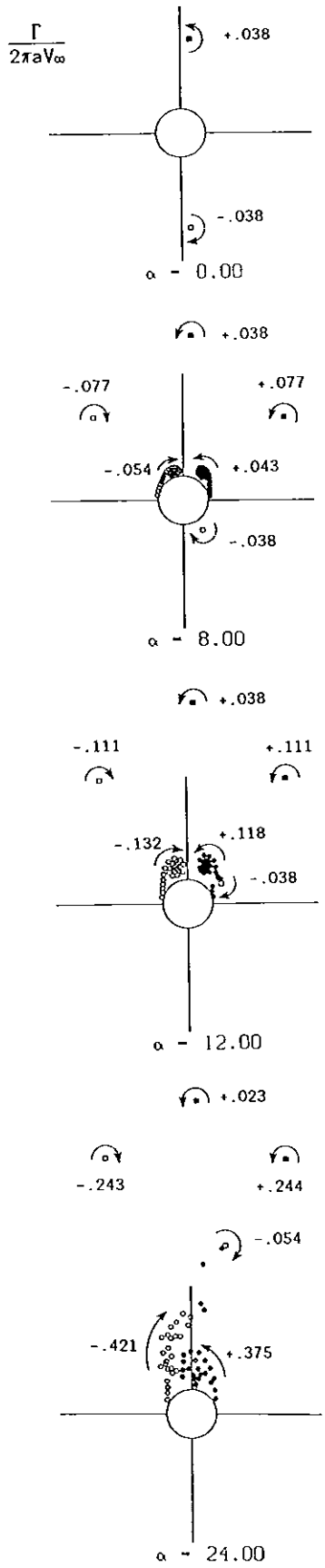

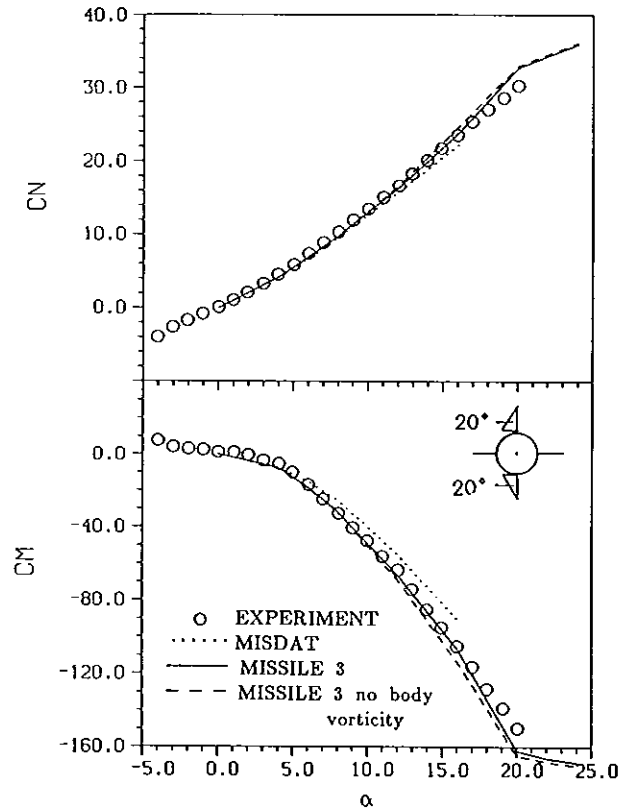

(a) Longitudinal Characteristics

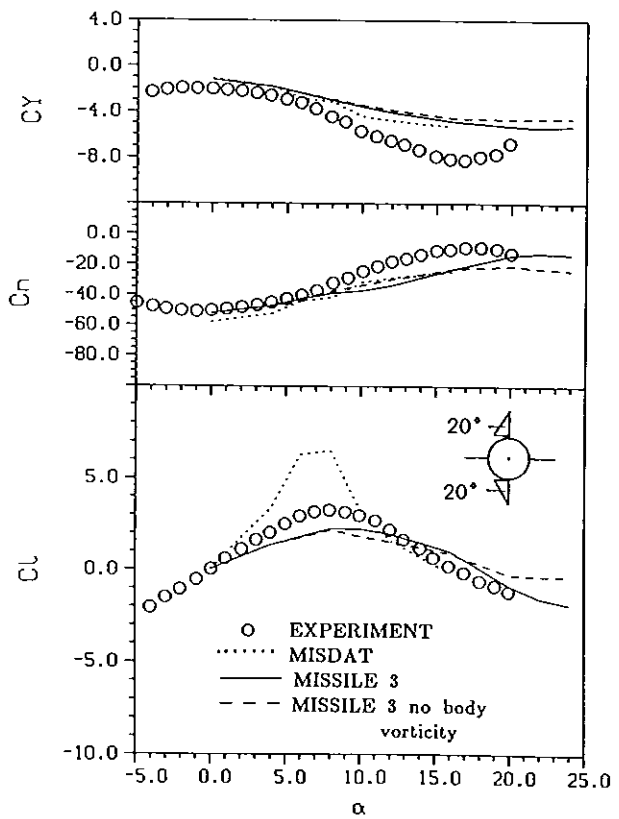

(b) Lateral-Directional Characteristics

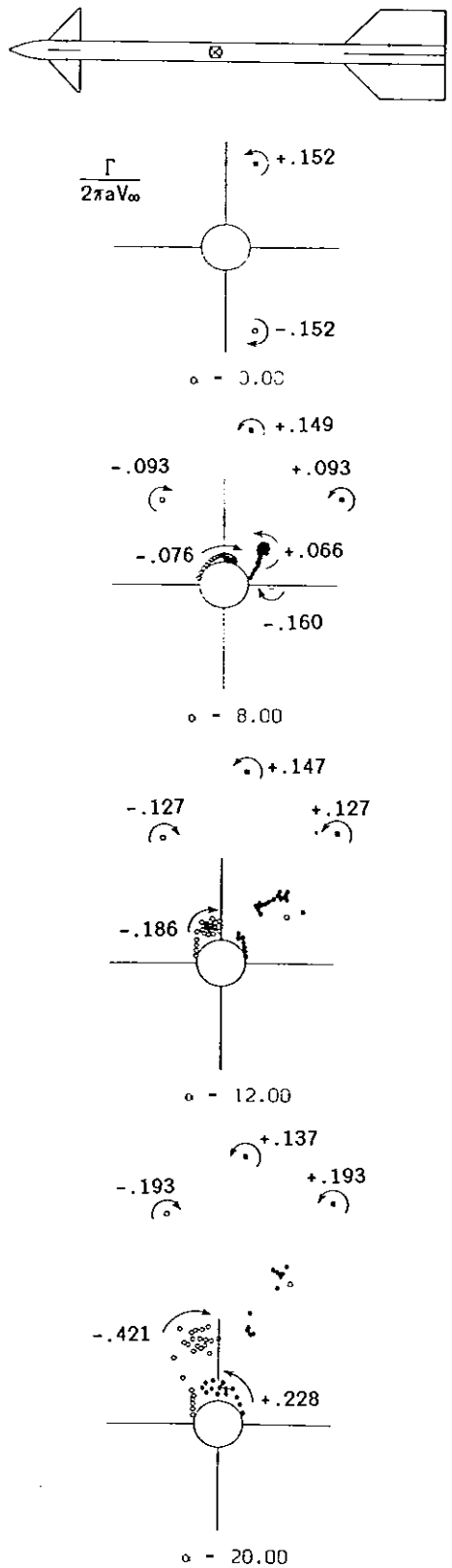

Figure 12.- Comparison of predicted and measured aerodynamic characteristics for the canard-body-tail model in Ref. 13, $M_\infty = 0.8$, $\phi = 0°$, $\delta_{1,3} = 20°$ yaw control.

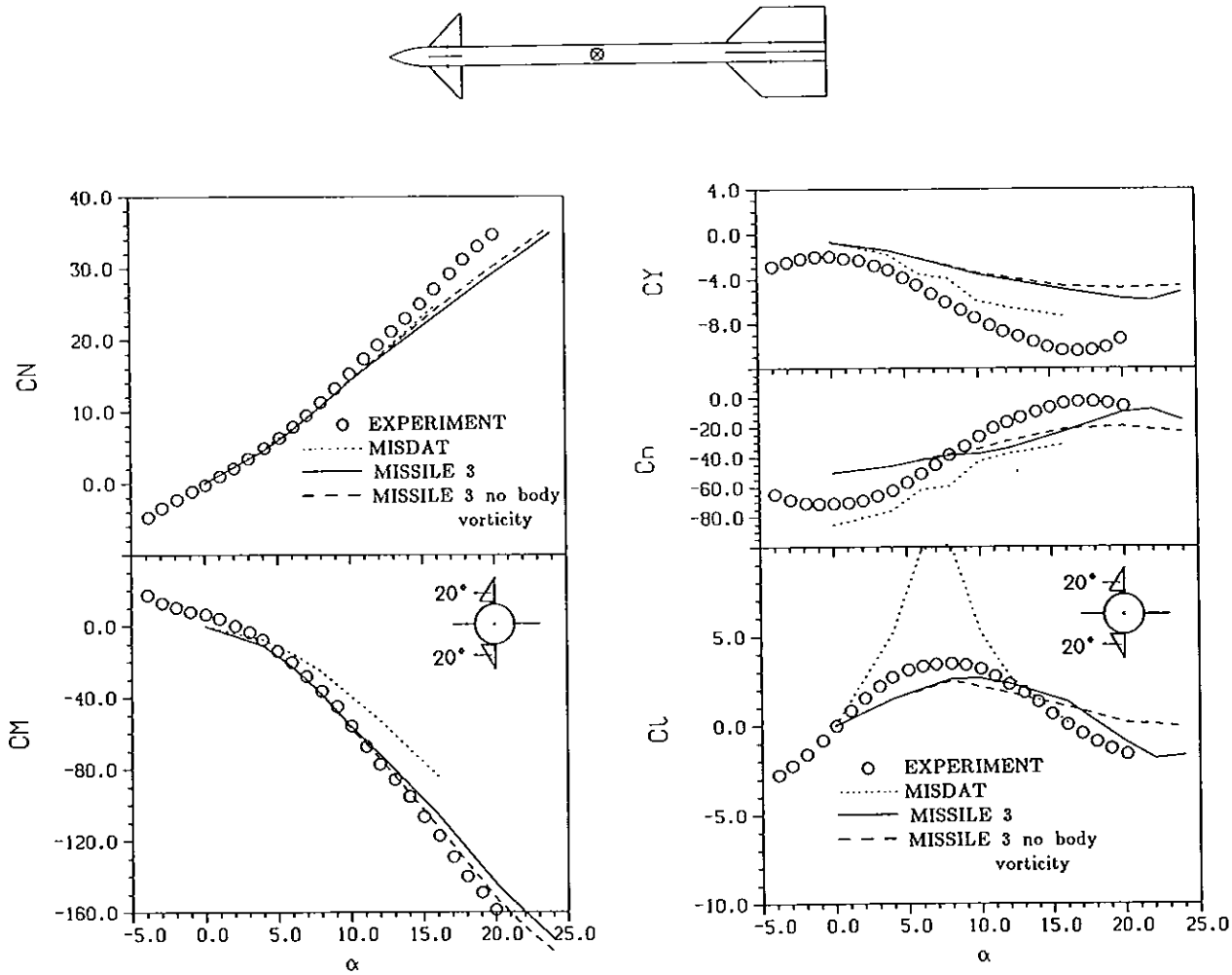

(a) Longitudinal Characteristics

(b) Lateral-Directional Characteristics

Figure 13.- Comparison of predicted and measured aerodynamic characteristics for the canard-body-tail model in Ref. 13, $M_\infty = 1.14$, $\phi = 0°$, $\delta_{1,3} = 20°$ yaw control.